Functional and structural architecture of the human dorsal frontoparietal attention network

Sara M. Szczepanski[a,b], Mark A. Pinsk[a,b], Malia M. Douglas[c], Sabine Kastner[a,b], and Yuri B. Saalmann[a,b,1]

Departments of [a]Psychology and [c]Electrical Engineering and [b]Princeton Neuroscience Institute, Princeton University, Princeton, NJ 08540

Edited by Leslie G. Ungerleider, National Institute of Mental Health, Bethesda, MD, and approved August 16, 2013 (received for review July 23, 2013)

The dorsal frontoparietal attention network has been subdivided into at least eight areas in humans. However, the circuitry linking these areas and the functions of different circuit paths remain unclear. Using a combination of neuroimaging techniques to map spatial representations in frontoparietal areas, their functional interactions, and structural connections, we demonstrate different pathways across human dorsal frontoparietal cortex for the control of spatial attention. Our results are consistent with these pathways computing object-centered and/or viewer-centered representations of attentional priorities depending on task requirements. Our findings provide an organizing principle for the frontoparietal attention network, where distinct pathways between frontal and parietal regions contribute to multiple spatial representations, enabling flexible selection of behaviorally relevant information.

parietal cortex | frontal cortex | DTI | fMRI | connectivity

Visual scenes usually contain many different objects, which cannot all be processed simultaneously because of the limited capacity of the visual system. Attention mechanisms are thus needed to select the most behaviorally relevant information for further processing. Previous studies have demonstrated activations over large portions of dorsal frontoparietal cortex during a variety of selective attention tasks (1, 2). In humans, these regions include intraparietal sulcus areas 1–5 (IPS1–IPS5) and superior parietal lobule area 1 (SPL1) in posterior parietal cortex (PPC), defined by spatial topographic mapping (3, 4), as well as the frontal eye field (FEF) and the putative human supplementary eye field (SEF) in frontal cortex (Fig. S1). Although these areas are commonly conceptualized as a frontoparietal attention network, the circuitry linking areas, the functions of different circuit paths, and the different roles of individual areas in representing attentional priorities remain unclear.

Because everyday actions rely on representations of attentional priorities in egocentric (gaze-centered, body-centered) and allocentric (object-centered, world-centered) spatial reference frames (5–9)—for example, to pick up a coffee cup, we must know where the cup is relative to our body, as well as where the handle is relative to the cup—we need to flexibly specify and read out attentional priorities in different reference frames. However, human neuroimaging studies have largely focused on gaze-centered representations and have been relatively unsuccessful in finding representations in other spatial reference frames, perhaps because they have focused on visual cortex (e.g., refs. 10 and 11). In frontoparietal cortex, the topographic organization of IPS1-5, SPL1, and FEF suggests that they contain spatial representations at least in egocentric reference frames (3, 12, 13). In contrast, human SEF lacks a clear topography (Fig. S1; refs. 14–16). Macaque SEF also lacks a clear topography (17, 18), although macaque SEF neurons have been shown to represent space in gaze-centered as well as head-, body-, and object-centered reference frames (9, 19). This diversity in macaque SEF neuronal responses suggests that the human SEF may be able to represent space in multiple reference frames as well.

Different inputs from IPS1-5 and SPL1 may contribute to the difference in functional organization between the FEF and SEF. In macaque monkeys, PPC subdivisions contain different proportions of neurons representing space in egocentric, allocentric, or intermediate reference frames (20–24). Computational studies have shown that it is possible to combine outputs from such neurons to perform different spatial transformations (25). Thus, distinct pathways from parietal areas to frontal cortex could give rise to the representation of attentional priorities in a number of different reference frames. Analyzing functional and structural connectivity in frontoparietal circuits might therefore be a useful approach to study different spatial representations. Here, we used a combination of topographic mapping, functional connectivity analyses of functional magnetic resonance imaging (fMRI) data, and structural connectivity analyses using diffusion MRI (dMRI) to test the hypotheses that: (*i*) there are distinct functional pathways within the dorsal frontoparietal attention network, (*ii*) these pathways support different spatial representations of attentional priorities, and (*iii*) structural connectivity between dorsal frontal and parietal areas supports this functionality. Our findings demonstrate that the FEF and SEF form distinct pathways to parietal areas, consistent with roles in enabling the specification and readout of attentional priorities in egocentric and allocentric reference frames.

Results

Two Pathways in the Dorsal Frontoparietal Attention Network. In our first study, we investigated whether different functional pathways exist between FEF/SEF and PPC. fMRI data were acquired while subjects performed a motion detection task (Fig. 1*A*). In this task, subjects were cued to direct and maintain attention to the right or left visual field (RVF, LVF) in expectation of moving, chromatic dots appearing in the periphery. Subjects responded when the dots moved in a particular target direction (see *SI Materials and Methods* for details). For each hemisphere and subject, the functional connectivity between time series derived from frontoparietal regions of interest (ROIs) was calculated

Significance

Everyday actions require us to represent attentional priorities in different reference frames. For example, to pick up a cup of coffee, we need to know where the cup is relative to our body, and where the handle is relative to the cup (i.e., body-centered and object-centered reference frames). Multiple brain areas in frontal and parietal cortex help process attentional priorities. Although these areas are commonly conceptualized as an attentional network, it is not clear what neural pathways connect these areas, nor the pathways' functions. We demonstrate that two pathways link these areas in frontal and parietal cortex. The pathways help represent attentional priorities in different reference frames, enabling us to flexibly interact with objects in our environment.

Author contributions: S.M.S., S.K., and Y.B.S. designed research; S.M.S., M.A.P., and Y.B.S. performed research; S.M.S., M.A.P., M.M.D., and Y.B.S. analyzed data; and S.M.S., S.K., and Y.B.S. wrote the paper.

The authors declare no conflict of interest.

This article is a PNAS Direct Submission.

[1]To whom correspondence should be addressed. E-mail: saalmann@princeton.edu.

This article contains supporting information online at www.pnas.org/lookup/suppl/doi:10.1073/pnas.1313903110/-/DCSupplemental.

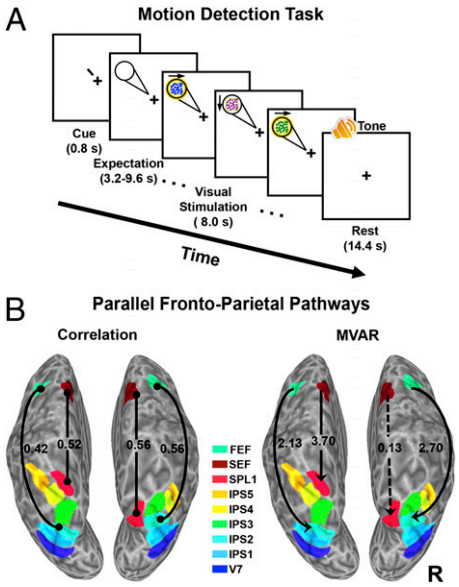

Fig. 1. Two pathways in the dorsal frontoparietal attention network. (*A*) Subjects were cued to covertly attend to the RVF or LVF in expectation of the motion stimulus for the motion detection task. (*B*) Functional connectivity analyses showed a lateral pathway connecting FEF to IPS2, and a medial pathway connecting SEF to SPL1, when subjects attended to the contralateral visual field, but not to the ipsilateral visual field, during the expectation period. Solid lines denote significant correlations (correlation analysis; *Left*) and solid arrows denote the direction of significant causal influence (MVAR; *Right*) between frontal and PPC areas, for the group of subjects. Dotted line denotes connection that is not statistically significant. Frontoparietal areas are color coded (designated by color key).

for a full model that included IPS1–5, SPL1, FEF, and SEF. This model was narrowed to IPS1, IPS2, SPL1, FEF, and SEF, because areas IPS3–5 did not significantly interact with the other frontoparietal areas when incorporated into the extended model. We used two measures of functional connectivity, correlation analysis and multivariate autoregressive (MVAR) modeling, to cross-check results. Two task conditions were analyzed in this study: (*i*) the expectation condition (Fig. 1*A*), in which subjects allocated attention to the periphery of the RVF or LVF before the appearance of a target stimulus (see Fig. S2 for focused spatial attention effects on BOLD responses from individual visual areas), and (*ii*) the unattended control condition, in which the same moving dot stimuli eventually appeared on the screen, but subjects received no prior attentional cues and were not anticipating or attending to the peripheral targets (*Materials and Methods*). Subjects detected on average 83.7 ± 1.8% of the targets presented in the RVF and 82.9 ± 1.4% of the targets presented in the LVF, confirming that subjects attended to the cued locations. Subjects detected 98.6 ± 0.4% of the luminance changes at fixation during the unattended condition, confirming that they ignored the peripheral stimuli when instructed to do so.

The correlation analysis across the group of subjects ($n = 7$) revealed differential connectivity of the FEF and SEF with parietal areas. For the group, the correlation between FEF and IPS2 was significantly greater during periods when subjects attended to the contralateral visual field [right hemisphere (RH): $r = 0.56$; left hemisphere (LH): $r = 0.42$; Fig. 1*B, Left*] than when they attended to the ipsilateral visual field (RH: $r = 0.44$; LH: $r = 0.25$) (paired t test; RH: $P = 0.023$; LH: $P = 0.035$). The group correlation between SEF and SPL1 was also significantly greater when subjects attended to the contralateral (RH: $r = 0.56$; LH: $r = 0.52$; Fig. 1*B, Left*) than to the ipsilateral (RH: $r = 0.43$; LH: $r = 0.44$) visual field (t test; RH: $P = 0.01$; LH: $P = 0.019$). Consistent with the correlation analysis results, MVAR showed that the FEF and SEF influenced different parietal areas (Fig. 1*B, Right*). The causal influence from FEF to IPS2 was significantly greater when subjects attended to the contralateral than to the ipsilateral visual field (t test; RH: $P = 0.018$; LH: $P = 0.039$). In addition, the causal influence from SEF to SPL1 was significantly greater during attention to the contralateral than to the ipsilateral visual field in the LH, but not in the RH (t test; RH: $P = 0.45$; LH: $P = 0.005$). There were no areas whose connectivity was stronger during attention to the ipsilateral than contralateral visual field ($P > 0.10$). None of the significantly stronger connections during expectation to the contralateral than ipsilateral visual field were significant in the unattended control condition ($P > 0.10$), suggesting that these frontoparietal interactions depend on active allocation of attention. Overall, these results suggest that there may be at least two dorsal pathways between frontal cortex and PPC involved in spatial attention processing: a lateral projection connecting FEF to IPS2 and a medial projection connecting SEF to SPL1.

Flexible Object-Centered and Gaze-Centered Representations in Frontoparietal Pathways. The FEF-IPS2 and SEF-SPL1 pathways in the first study may have represented space in a gaze-centered (i.e., in relation to the fixation point) or an object-centered (i.e., in relation to the screen) reference frame. In addition to gaze-centered neurons, the macaque SEF contains neurons that represent space in an object-centered reference frame (9). In our second study, we thus investigated whether the SEF-SPL1 pathway could use a different reference frame, specifically an object-centered representation, for attentional priorities. We tested this hypothesis directly in a second fMRI study by using a pattern detection task (Fig. 2*A*; ref. 15), which allowed us to dissociate the effects of viewer-centered and object-centered spatial attention. In attended conditions of this task, four patterned tiles grouped into a large square appeared in the periphery (RVF or LVF) and subjects paid attention to the tile closest to fixation, counting targets that appeared in this location (on the left or right side of the large square; see *SI Materials and Methods* for details). In the unattended conditions, the identical visual stimuli appeared in the periphery, but subjects ignored them and instead performed a letter-counting task at fixation.

We designed the task such that subjects attended to the contralateral side of the large square when it was in the ipsilateral visual field, or to the ipsilateral side of the large square when it was in the contralateral visual field. This manipulation was done because monkey electrophysiology has shown that many neurons showing object-centered responses represent the contralateral side of an object (9). We thus hypothesized that there should be greater connectivity between SEF and SPL1 when the large square was in the ipsilateral visual field (corresponding to attention to the contralateral side of the large square) if this pathway represented object-centered information. Subjects detected on average 88.1 ± 2.1% of the targets presented in the RVF and 91.2 ± 1.9% of the targets presented in the LVF, confirming that they attended to the appropriate part of the large square.

For each hemisphere and subject ($n = 13$) in the pattern detection task, we again used a correlation analysis to determine significant connections among IPS1, IPS2, SPL1, FEF, and SEF. An omnibus ANOVA of the correlation coefficients revealed a significant attention (attended vs. unattended) × connection (FEF-IPS2 vs. SEF-SPL1) × visual field (contralateral vs. ipsilateral) interaction, $F_{(1,12)} = 6.30$, $P < 0.05$. This three-way interaction was driven by a connection × visual field interaction that was significant in the attended conditions, $F_{(1,12)} = 22.93$, $P < 0.001$, but not significant in the unattended control conditions, $F_{(1,12)} = 0.47$, $P > 0.50$. More specifically, for the group, the correlation between FEF and IPS2 was larger during periods when subjects attended to the contralateral visual field/ipsilateral side of the large square (RH: $r = 0.59$; LH: $r = 0.52$; Fig. 2*B, Left*) than when they attended to the ipsilateral visual field/contralateral side of the large square (RH: $r = 0.47$; LH: $r = 0.40$) (t test; RH: $P = 0.022$; LH: $P = 0.042$), consistent with the motion detection task results reported above. In contrast, the group correlation

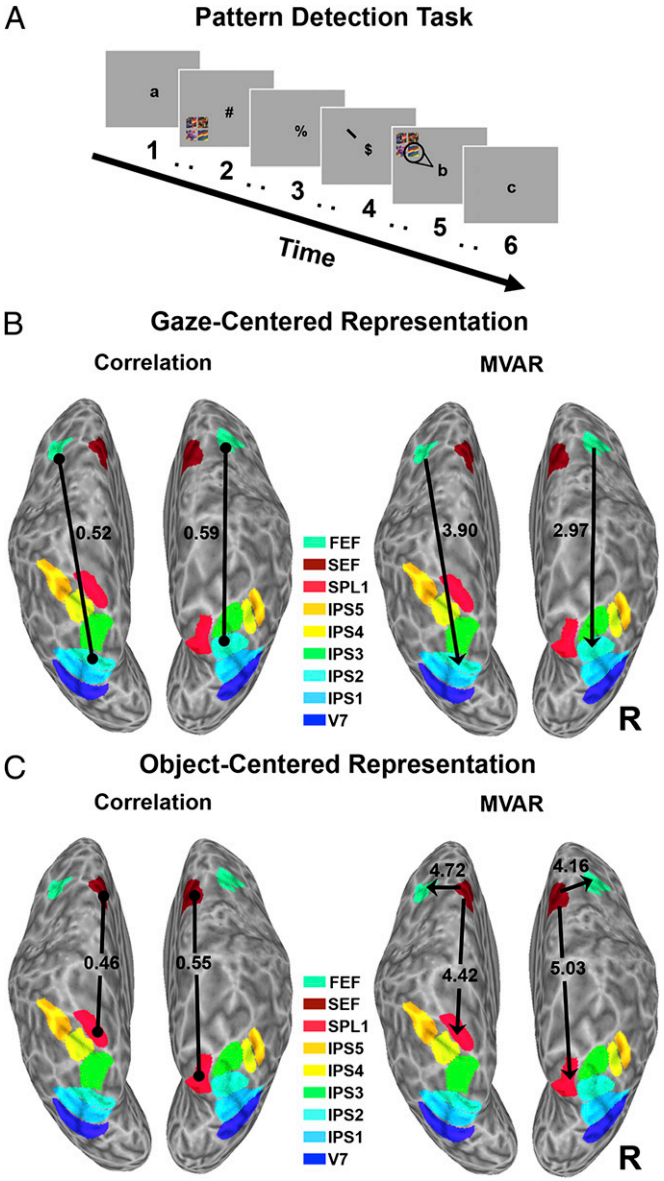

Fig. 2. Object-centered and gaze-centered representations in frontoparietal pathways. (*A*) For the pattern detection task, subjects were cued to the location of an upcoming stimulus comprising four patterned tiles arranged as a large square, and they covertly attended to the tile in the section of the square closest to the fixation point. For the unattended control, there was no cue, so subjects ignored the tiles and instead counted letters at fixation. (*B*) Significant correlations (*Left*) and causal influences (MVAR; *Right*) between frontoparietal ROIs when subjects attended to the contralateral visual field/ipsilateral side of the large square. (*C*) Significant correlations (*Left*) and causal influences (MVAR, *Right*) between frontoparietal ROIs when subjects attended to the ipsilateral visual field/contralateral side of the large square. Frontoparietal areas are color-coded.

between SEF and SPL1 was larger during periods when subjects attended to the ipsilateral visual field/contralateral side of the large square (RH: $r = 0.55$; LH: $r = 0.46$; Fig. 2*C, Left*) than when they attended to the contralateral visual field/ipsilateral side of the large square (RH: $r = 0.44$; LH: $r = 0.26$) (t test; RH: $P = 0.034$; LH: $P = 0.039$).

MVAR showed a similar pattern of frontoparietal connectivity. The omnibus ANOVA of the path coefficients revealed a significant attention × connection × visual field interaction, $F_{(1,12)} = 9.73$, $P < 0.01$. This three-way interaction was again due to a significant connection × visual field interaction in the attention conditions, $F_{(1,12)} = 8.77$, $P < 0.01$, that was not significant in the unattended control condition, $F_{(1,12)} = 1.95$, $P > 0.10$. When subjects attended to the contralateral visual field, FEF significantly influenced IPS2 in both hemispheres (t test; RH: $P = 0.011$; LH: $P = 0.002$; Fig. 2*B, Right*), whereas there was no significant influence between SEF and SPL1 in either hemisphere ($P > 0.05$). In contrast, when subjects attended to the ipsilateral visual field, SEF causally influenced SPL1 (t test; RH: $P = 0.0003$; LH: $P = 0.0008$) and the FEF (RH: $P = 0.001$; LH: $P = 0.0005$; Fig. 2*C, Right*), but there was no significant influence between FEF and IPS2 in either hemisphere ($P > 0.10$). None of the same connections that were significantly stronger during contralateral than ipsilateral attention were significant in the unattended control condition, during which subjects ignored the object ($P > 0.05$). Overall, these results suggest that the SEF-SPL1 pathway conveyed object-centered representations of spatial attention priorities, whereas the FEF-IPS2 pathway used viewer-centered representations, in the pattern detection task.

Robust Structural Connections Between FEF and IPS2 and Between SEF and SPL1. In a third study, we aimed to identify structural connections in support of the FEF-IPS2 and SEF-SPL1 pathways, using probabilistic tractography of dMRI data in 14 subjects who participated in the motion or pattern detection tasks. The probabilistic tractography results showed robust frontoparietal connections (26), including the FEF-IPS2 and SEF-SPL1 pathways, consistent with the functional connectivity results. Fig. 3 *A* and *B* show probable fiber tracks between frontal cortex and IPS2 or SPL1, respectively, for an individual subject. In both hemispheres, IPS2 had a significantly higher proportion of connections with the FEF than SPL1 had with the FEF [t test; RH: $P = 0.0015$, LH: $P = 0.0017$; group mean proportion of probabilistic streamlines from IPS2 to FEF (vs. SEF): RH: 83.8 ± 4.7%, LH: 82.6 ± 4.0%]. In contrast, SPL1 had a significantly higher proportion of connections with the SEF than IPS2 had with the SEF [t test; RH: $P = 0.0073$, LH: $P = 0.0032$; group mean proportion of probabilistic streamlines from SPL1 to SEF (vs. FEF): RH: 42.8 ± 7.2%, LH: 43.3 ± 6.7%]. We next classified each voxel in IPS2 and SPL1 based on whether it had a higher connection probability with the FEF or SEF (hard segmentation). Fig. 3*C* shows the hard segmentation of IPS2 for an individual subject, and Fig. 3*E* shows the group hard segmentation derived from a conjunction analysis of each individual's hard segmented IPS2. Nearly all of the IPS2 voxels were preferentially connected to the FEF (group mean proportion of FEF-preferring voxels from hard segmentations: RH: 85.4 ± 6.4%, LH: 89.6 ± 3.9%). Fig. 3 *D* and *F* show the hard segmentation of SPL1 for an individual and the group, respectively. SPL1 could be divided into two regions based on its frontal connectivity pattern. Lateral SPL1 voxels were preferentially connected to the FEF, whereas medial voxels were preferentially connected to the SEF (Fig. 3*F*; group mean proportion of SEF-preferring voxels from hard segmentations: RH: 32.9 ± 8.7%, LH: 49.3 ± 14.9%). For six of eight subjects who participated in both pattern detection and dMRI experiments, the SPL1 attention activation (functional ROI) overlapped with the SEF-projection zone (structural ROI; Fig. S3). These results suggest that neurons contributing to different spatial representations may be unevenly distributed across SPL1.

Discussion

The topographic mapping, functional connectivity, and structural connectivity results converge to provide evidence for the existence of distinct pathways across dorsal frontoparietal cortex. Further, the fMRI results are consistent with these pathways giving rise to the representation of attentional priorities in multiple spatial reference frames: a viewer-centered pathway between FEF and IPS2, and a more flexible pathway between SEF and SPL1 supporting object- and viewer-centered representations. Such flexibility in spatial representations enables condition-action associations, which are a hallmark of the SEF

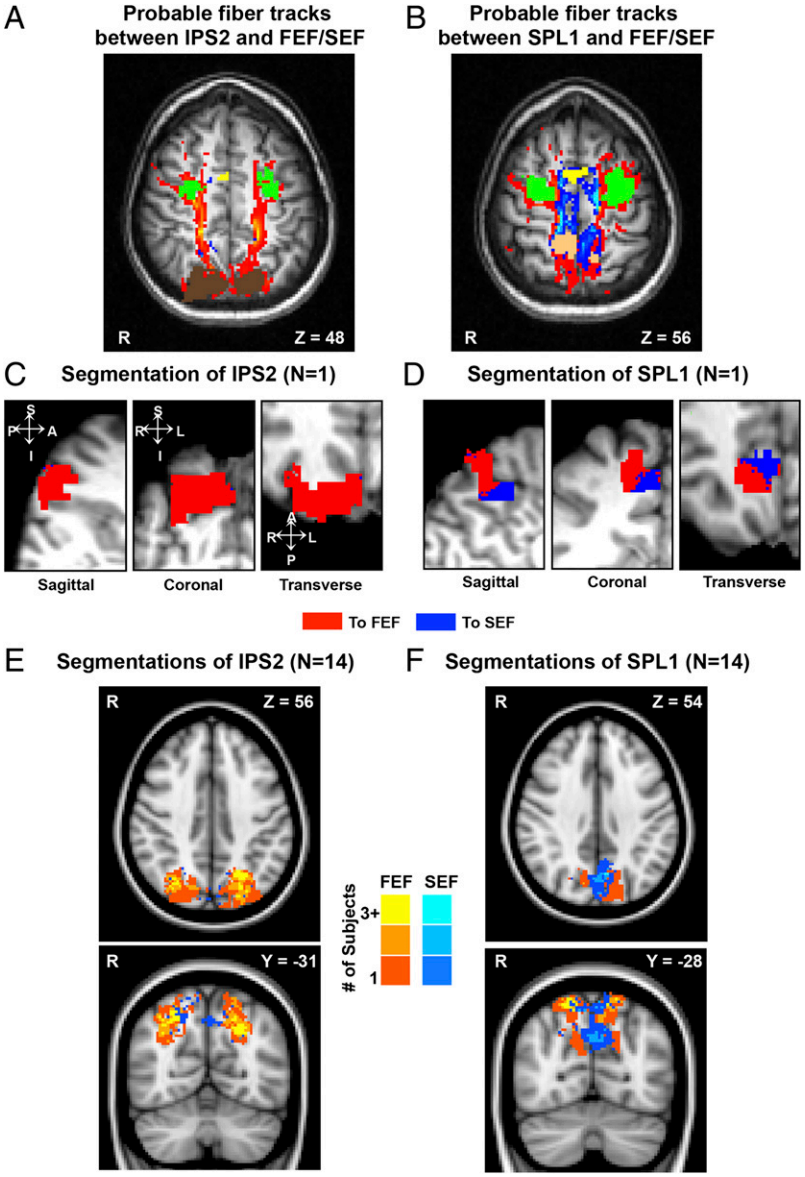

Fig. 3. Structural connectivity between IPS2-FEF and SPL1-SEF/FEF. (*A*) Probable fiber tracts between IPS2 (brown) and FEF (green) or SEF (yellow), in a typical subject (same subject in *A*–*D*). Probability is color-coded (higher-lower) for IPS2-FEF (orange-red) and IPS2-SEF (light blue-dark blue). (*B*) Probable fiber tracts between SPL1 (pink) and FEF or SEF. Probability was color-coded (higher-lower) for SPL1-FEF (orange-red) and SPL1-SEF (light blue-dark blue). (*C*) Segmentation of right IPS2 in an example subject, shown in sagittal (*Left*), coronal (*Center*), and transverse (*Right*) slices. Red voxels preferentially connect to the FEF, whereas blue voxels preferentially connect to the SEF. (*D*) Segmentation of right SPL1 in the same subject. Conventions as in *C*. (*E*) Group segmentation of IPS2 derived from a conjunction analysis of the 14 subjects' IPS2 data (axial view, *Upper*; coronal view, *Lower*). Voxels are color-coded based on whether they preferentially connect with FEF (orange-yellow scale) or SEF (blue scale). The lighter the color, the higher the number of overlapping subjects. (*F*) Group segmentation of SPL1. Conventions as in *E*.

and supplementary motor cortex in general (27), as well as task-switching, in which the SEF and SPL play prominent roles (28, 29). In comparison, evidence suggests that the FEF and IPS contain a salience map in gaze-centered coordinates that helps guide exploration of the visual environment (16, 30, 31), consistent with our mapping of the FEF-IPS2 pathway. In addition to using the FEF-IPS2 and SEF-SPL1 pathways to guide eye movements and provide attentional feedback to sensory areas, these pathways may act in concert to remap space across saccades, considering that the relative positions of objects and viewer-centered information help maintain visual stability (32).

Numerous studies have demonstrated that the FEF and portions of the IPS in both the human and the monkey are essential for the control of spatial attention (1, 30, 31). In contrast, much less is known about how SEF and SPL contribute to spatial attention control. Although macaque SEF is known to represent attentional priorities in multiple reference frames, including object-centered representations, the human SEF has only been shown to respond strongly during spatial attention in an egocentric reference frame (9, 14, 15). Here we provide evidence consistent with a role of human SEF in object-centered attention, similar to macaque SEF. We demonstrated that SPL1 responds robustly during spatial attention (15) and here, we now implicate SPL1 in object-centered and gaze-centered representations. This result is consistent with previous studies showing overlapping activations for egocentric and allocentric processing in superior and medial parietal cortex (33, 34). Furthermore, a portion of the SPL is "transiently" active during voluntary shifts of attention between locations, features, and objects (35). Based on published coordinates (e.g., RH: $x = +11$, $y = -60$, $z = +55$; ref. 36), it appears that there is partial overlap between this region showing transient responses and SPL1, with SPL1 extending more posteriorly (RH: $x = +9$, $y = -73$, $z = +43$; ref. 15). The transient activity had been interpreted to be spatially nonspecific in the context of gaze-centered representations of space (36). However, an alternative interpretation is possible if the SPL contributes to spatial representations in multiple reference frames: The transient activity could be spatially specific if it represented attentional shifting between spatial representations in different reference frames (e.g., object- to gaze-centered, object1- to object2-centered).

We found large responses in the SEF and SPL1 when subjects attended to the ipsilateral visual field while performing the pattern detection task (15), consistent with the hypothesis tested

in the current study that these areas contribute to object-centered spatial representations. Here, SEF and SPL1 were significantly connected only when stimuli were attended in the visual field ipsilateral to each hemisphere, but not when stimuli were attended in the visual field contralateral to each hemisphere, while subjects performed the pattern detection task. If SEF and SPL1 were only representing space in viewer-centered coordinates during the pattern detection task, a significant connection between the two areas should have also existed when subjects attended to the contralateral visual field. Rather, our results more strongly support the interpretation that SEF and SPL1 are able to flexibly represent space in viewer-centered or object-centered coordinates, depending on task requirements. Such flexibility might arise from a population of neurons representing a range of reference frames, including intermediates between gaze-centered and object-centered reference frames (20, 24), whose output can be differentially combined to support multiple spatial representations. In this regard, the functional connectivity analyses were able to reveal distinct spatial transformations across frontoparietal cortex. Flexible representation of space using different reference frames according to context may be common in frontal and parietal areas, with a recent study reporting flexible gaze- and body-centered representations in parietal area BA5 and dorsal premotor cortex (37).

Human neuroimaging and monkey physiology studies have traditionally examined various frontal and parietal areas in isolation, rather than focusing on how these areas function as a network to subserve spatial attention. Although the functions of various subdivisions of monkey PPC and their connectivity patterns are better understood, comparatively little is known about the functional characteristics and connectivity patterns of various subdivisions within human PPC. dMRI has been used to study the structural connectivity of human PPC (26, 38), but it has not been combined with topographic mapping to show the specific connections of IPS1-5 and SPL1 with frontal cortical areas. The anatomical connections that we have identified by using dMRI are similar to the anatomical connections that have been identified between frontal and parietal cortex in the macaque (39): An area within macaque IPS (lateral intraparietal area) was heavily connected with the FEF, similar to our FEF-IPS2 connection, whereas a medial region of macaque PPC was connected with both the SEF and the FEF, similar to our SEF/FEF-SPL1 connections.

In conclusion, the combination of topographic mapping, dMRI, and functional connectivity analyses has provided evidence of separate pathways for the control of spatial attention across human dorsal frontoparietal cortex. These pathways support different spatial representations of attentional priorities, including likely gaze-centered and object-centered representations. We propose that other parietal areas, such as IPS3–5, may form further pathways enabling flexible specification and readout of behaviorally relevant information in additional reference frames (e.g., body-centered or world-centered coordinates).

Materials and Methods

Subjects. Twenty-one healthy subjects (25–36 y, seven females) gave informed written consent to participate in the study, approved by the Institutional Review Panel of Princeton University. All subjects had normal or corrected-to-normal vision.

Data Acquisition. ***Echo-planar imaging.*** We acquired data by using a 3T Allegra MRI scanner (Siemens) with a Nova transmit and receive head coil (Nova Medical) for the motion detection task [8 subjects, 26 transverse slices, slice thickness 3 mm, interslice gap 1 mm, repetition time (TR) 1.6 s, echo time (TE) 40 ms, flip angle 72°, in-plane resolution 3 × 3 mm, 2,240 volumes], pattern detection task (13 subjects, 20 transverse slices, slice thickness 2 mm, interslice gap 1 mm, TR 2 s, TE 41 ms, flip angle 90°, in-plane resolution 2 × 2 mm, 1,248 volumes), and memory-guided saccade task (21 subjects, 25 transverse slices, slice thickness 2 mm, interslice gap 1 mm, TR 2.5 s, TE 41 ms, flip angle 90°, in-plane resolution 2 × 2 mm, 1,152 volumes). In-plane gradient echo field map images and magnitude images were acquired to perform geometric unwarping on the high-resolution echo-planar imaging (EPI) images (TR 345 ms, TE 5.06/8.06 ms, flip angle 40°, bandwidth 260 Hz per pixel). We aligned all echo-planar images to a high-resolution anatomical scan taken at the end of each session (MPRAGE sequence, 256 × 256 matrix, TR 2.5 s, TE 4.38 s, flip angle 8°, 1 mm^3 resolution). Six high-resolution anatomical scans were also acquired in a separate session and averaged to create cortical surface reconstructions.

dMRI. We acquired diffusion-weighted images (DWI) by using an eddy-current compensated double spin-echo, echo-planar pulse sequence (40). Images with 2.0 mm^3 resolution were collected by using 60 different isotropic diffusion directions (41) (14 subjects, 66 contiguous transverse slices, anterior to posterior phase-encode direction, 128 × 128 matrix, slice thickness 2.0 mm, TR 10 s, TE 95 ms, interleaved acquisition, *b* values 0 and 1,000 s/mm^2, 1,776 Hz per pixel bandwidth, 0.61 ms echo spacing). We used a 12:1 ratio of DWI to non-DWI images (41, 42) and cardiac gating to minimize artifacts due to pulsatile motion (43). A total of six 60-direction sets of diffusion-weighted data were acquired for subsequent averaging. We also acquired gradient echo field maps and magnitude images with slice prescriptions identical to the diffusion-weighted images to perform geometric unwarping during preprocessing (TR 500 ms, TE 5.23/7.69 ms, flip angle 55°, 1,502 Hz per pixel bandwidth). All diffusion-weighted images were aligned to a high-resolution anatomical scan taken at the end of each session.

Data Analysis. ***Defining ROIs.*** We defined ROIs based on the intersection of topographic maps (FEF, IPS1-5, and SPL1) and attention activations in each subject ($n = 21$). See *SI Materials and Methods* for details.

Functional connectivity. We extracted raw fMRI signals from the slice time-corrected and motion-corrected EPI images. Two sources of variance were removed through linear regression: six parameters obtained by rigid body correction of head motion and global mean signal changes. We next low-pass filtered (<0.20 Hz) and linearly detrended the time series, smoothed with a 4-mm Gaussian kernel, standardized the signals, and then averaged across all voxels within a given ROI. ROIs were defined as the voxel with the peak attention activity in each topographic area of each hemisphere and the six surrounding voxels in the *x*, *y*, and *z* directions. We modeled each hemisphere, attended and unattended conditions separately. For the motion detection task, we analyzed timepoints during the expectation periods (8 s mean span, shifted 2 TRs after cue) that immediately preceded the moving dot stimuli in the attended condition. We modeled the equivalent timepoints for the unattended condition, although no cue was presented. For the pattern detection task, we used all timepoints in each block except for the first TR, analyzing attended and unattended conditions similarly.

For correlation analyses, we first averaged the BOLD signal over volumes in each block to generate one sample point in a discontinuous time series for each ROI; repeating this procedure for every block generated the full-time series (44). We next calculated the Pearson's correlation coefficient for all ROI pairs in each subject (45) and Fisher transformed these coefficients. For group analyses, we applied an omnibus repeated-measures ANOVA to the Fisher-transformed coefficients from each subject with attention (attended vs. unattended), hemisphere (RH vs. LH), connection (FEF-IPS2 vs. SEF-SPL1), and visual field (contralateral vs. ipsilateral) as factors. We followed with ANOVAs applied separately to the attended and unattended conditions and one-tailed paired *t* tests. To control for multiple comparisons, we used the false discovery rate ($q = 0.05$) approach, and significant connections satisfied the criterion of being significant in both hemispheres. For MVAR (46) of each subject, we used a model order of 2 for the motion detection task, and a model order of 1 for the pattern detection task, based on the Akaike information criterion. Model quality checks were run to assess data normality (Jarque–Bera Test) and stationarity [autoregressive conditional heteroskedasticity (ARCH) test] for each individual subject. For group analyses, we applied an omnibus repeated-measures ANOVA to the path coefficients derived from the individual subject analyses by using the same factors as above and followed with separate ANOVAs applied to the attended and unattended conditions and paired-sample *t* tests as planned comparisons.

Probabilistic tractography. All DWI and non-DWI images were corrected for eddy currents and head motion by using affine registration [12 degrees of freedom (DOF)] to a non-DWI reference volume, averaged to improve the signal-to-noise ratio, and geometrically unwarped (47). The skull-stripped anatomical volume was coregistered (12 DOF affine) to the averaged non-DWI reference volume to derive the transformation matrix between the two spaces. We conducted tractography by using The Oxford Center for Functional Magnetic Resonance Imaging of the Brain's (FMRIB's) Diffusion Toolkit (FDT), calculating probability distributions of fiber direction at each voxel (two fiber populations modeled per voxel) (48, 49).

First, we performed a tractography analysis to inspect probable paths passing through both the parietal and frontal ROIs for anatomical plausibility.

We used an exclusion mask to restrict our analyses to ipsilateral trajectories and a coronal waypoint mask midway between parietal and frontal ROIs to constrain trajectories to an anterior-posterior direction. We defined ROI pairs (IPS2-FEF, IPS2-SEF, SPL1-FEF, SPL1-SEF) in each hemisphere as ROI seeds for "multiple mask seed" tractography with FDT and thresholded the resulting pathways for each ROI pair to remove voxels containing fewer than 25 samples.

Second, we performed a tractography analysis to estimate pathways passing through any voxel in a single parietal seed and the probability such pathways will pass through a voxel in either of the two frontal targets ("single mask seed with classification targets" tractography with the FDT). From each seed voxel, 5,000 samples were drawn from the probability distribution (0.2 curvature threshold, 0.5-mm step length, distance corrected), and the proportion of these samples passing through each target equated to the probability of connection to that target. We used identical interhemispheric exclusion and coronal waypoint masks as above. We recorded the number of projections to a target area as a proportion of the total going to both targets. We next calculated the mean proportion of projections from each parietal seed to each frontal target by averaging all voxels in the seed area, allowing comparison between seeds (50). We performed repeated-measures ANOVAs, with factors for seed area and target area, followed by one-tailed paired-samples *t* tests for planned comparisons.

We hard segmented each seed area by classifying each seed voxel by the target mask to which it had the highest connection probability (48). To compare subjects' results, we performed a conjunction analysis on the IPS2 and SPL1 hard segmentations. First, we registered each subject's skull-stripped anatomical image to the MNI 152 template brain to create an affine transform matrix (12 DOF) for use during the nonlinear registration procedure. Next, using this transform matrix, a nonlinear warp transformation for each subject's original anatomical image was calculated and applied using FMRIB's Nonlinear Image Registration Tool. We applied the resulting nonlinear warp matrices to each subject's IPS2 and SPL1 hard segmentation by using nearest neighbor interpolation and overlaid on the MNI 152 template.

Eye Movement Recordings. We monitored eye movements during scanning sessions. See *SI Materials and Methods* for details.

ACKNOWLEDGMENTS. This study was supported by National Institutes of Health Grants R01MH64043, R01EY017699, and R21EY021078.

1. Kastner S, Ungerleider LG (2000) Mechanisms of visual attention in the human cortex. *Annu Rev Neurosci* 23:315–341.
2. Corbetta M, Shulman GL (2002) Control of goal-directed and stimulus-driven attention in the brain. *Nat Rev Neurosci* 3(3):201–215.
3. Silver MA, Kastner S (2009) Topographic maps in human frontal and parietal cortex. *Trends Cogn Sci* 13(11):488–495.
4. Sereno MI, Pitzalis S, Martinez A (2001) Mapping of contralateral space in retinotopic coordinates by a parietal cortical area in humans. *Science* 294(5545):1350–1354.
5. Behrmann M, Tipper SP (1999) Attention accesses multiple reference frames: Evidence from visual neglect. *J Exp Psychol Hum Percept Perform* 25(1):83–101.
6. Duncan J (1984) Selective attention and the organization of visual information. *J Exp Psychol Gen* 113(4):501–517.
7. Egly R, Driver J, Rafal RD (1994) Shifting visual attention between objects and locations: Evidence from normal and parietal lesion subjects. *J Exp Psychol Gen* 123(2): 161–177.
8. Mesulam MM (1999) Spatial attention and neglect: Parietal, frontal and cingulate contributions to the mental representation and attentional targeting of salient extrapersonal events. *Philos Trans R Soc Lond B Biol Sci* 354(1387):1325–1346.
9. Olson CR (2003) Brain representation of object-centered space in monkeys and humans. *Annu Rev Neurosci* 26:331–354.
10. Golomb JD, Chun MM, Mazer JA (2008) The native coordinate system of spatial attention is retinotopic. *J Neurosci* 28(42):10654–10662.
11. Golomb JD, Kanwisher N (2012) Higher level visual cortex represents retinotopic, not spatiotopic, object location. *Cereb Cortex* 22(12):2794–2810.
12. Pertzov Y, Avidan G, Zohary E (2011) Multiple reference frames for saccadic planning in the human parietal cortex. *J Neurosci* 31(3):1059–1068.
13. Sereno MI, Huang RS (2006) A human parietal face area contains aligned head-centered visual and tactile maps. *Nat Neurosci* 9(10):1337–1343.
14. Kastner S, et al. (2007) Topographic maps in human frontal cortex revealed in memory-guided saccade and spatial working-memory tasks. *J Neurophysiol* 97(5): 3494–3507.
15. Szczepanski SM, Konen CS, Kastner S (2010) Mechanisms of spatial attention control in frontal and parietal cortex. *J Neurosci* 30(1):148–160.
16. Van Pelt S, Toni I, Diedrichsen J, Medendorp WP (2010) Repetition suppression dissociates spatial frames of reference in human saccade generation. *J Neurophysiol* 104(3):1239–1248.
17. Schlag J, Schlag-Rey M (1987) Evidence for a supplementary eye field. *J Neurophysiol* 57(1):179–200.
18. Tehovnik EJ, Lee K (1993) The dorsomedial frontal cortex of the rhesus monkey: Topographic representation of saccades evoked by electrical stimulation. *Exp Brain Res* 96(3):430–442.
19. Martinez-Trujillo JC, Medendorp WP, Wang H, Crawford JD (2004) Frames of reference for eye-head gaze commands in primate supplementary eye fields. *Neuron* 44(6):1057–1066.
20. Chang SW, Snyder LH (2010) Idiosyncratic and systematic aspects of spatial representations in the macaque parietal cortex. *Proc Natl Acad Sci USA* 107(17):7951–7956.
21. Andersen RA, Bracewell RM, Barash S, Gnadt JW, Fogassi L (1990) Eye position effects on visual, memory, and saccade-related activity in areas LIP and 7a of macaque. *J Neurosci* 10(4):1176–1196.
22. Brotchie PR, Andersen RA, Snyder LH, Goodman SJ (1995) Head position signals used by parietal neurons to encode locations of visual stimuli. *Nature* 375(6528):232–235.
23. Snyder LH, Grieve KL, Brotchie P, Andersen RA (1998) Separate body- and world-referenced representations of visual space in parietal cortex. *Nature* 394(6696): 887–891.
24. Chafee MV, Averbeck BB, Crowe DA (2007) Representing spatial relationships in posterior parietal cortex: Single neurons code object-referenced position. *Cereb Cortex* 17(12):2914–2932.
25. Deneve S, Pouget A (2003) Basis functions for object-centered representations. *Neuron* 37(2):347–359.
26. Mars RB, et al. (2011) Diffusion-weighted imaging tractography-based parcellation of the human parietal cortex and comparison with human and macaque resting-state functional connectivity. *J Neurosci* 31(11):4087–4100.
27. Nachev P, Kennard C, Husain M (2008) Functional role of the supplementary and pre-supplementary motor areas. *Nat Rev Neurosci* 9(11):856–869.
28. Esterman M, Chiu YC, Tamber-Rosenau BJ, Yantis S (2009) Decoding cognitive control in human parietal cortex. *Proc Natl Acad Sci USA* 106(42):17974–17979.
29. Schall JD, Stuphorn V, Brown JW (2002) Monitoring and control of action by the frontal lobes. *Neuron* 36(2):309–322.
30. Goldberg ME, Bisley JW, Powell KD, Gottlieb J (2006) Saccades, salience and attention: The role of the lateral intraparietal area in visual behavior. *Prog Brain Res* 155: 157–175.
31. Thompson KG, Bichot NP (2005) A visual salience map in the primate frontal eye field. *Prog Brain Res* 147:251–262.
32. Prime SL, Vesia M, Crawford JD (2011) Cortical mechanisms for trans-saccadic memory and integration of multiple object features. *Philos Trans R Soc Lond B Biol Sci* 366(1564):540–553.
33. Fink GR, Dolan RJ, Halligan PW, Marshall JC, Frith CD (1997) Space-based and object-based visual attention: Shared and specific neural domains. *Brain* 120(Pt 11):2013–2028.
34. Committeri G, et al. (2004) Reference frames for spatial cognition: Different brain areas are involved in viewer-, object-, and landmark-centered judgments about object location. *J Cogn Neurosci* 16(9):1517–1535.
35. Serences JT, Liu T, Yantis S (2005) Parietal mechanisms of switching and maintaining attention to locations, objects, and features. *Neurobiology of Attention*, eds Itti L, Rees G, Tsotsos JK (Academic, New York), pp 35–41.
36. Yantis S, et al. (2002) Transient neural activity in human parietal cortex during spatial attention shifts. *Nat Neurosci* 5(10):995–1002.
37. Bernier PM, Grafton ST (2010) Human posterior parietal cortex flexibly determines reference frames for reaching based on sensory context. *Neuron* 68(4):776–788.
38. Anderson EJ, et al. (2012) Cortical network for gaze control in humans revealed using multimodal MRI. *Cereb Cortex* 22(4):765–775.
39. Cavada C, Goldman-Rakic PS (1989) Posterior parietal cortex in rhesus monkey: II. Evidence for segregated corticocortical networks linking sensory and limbic areas with the frontal lobe. *J Comp Neurol* 287(4):422–445.
40. Reese TG, Heid O, Weisskoff RM, Wedeen VJ (2003) Reduction of eddy-current-induced distortion in diffusion MRI using a twice-refocused spin echo. *Magn Reson Med* 49(1):177–182.
41. Jones DK, Horsfield MA, Simmons A (1999) Optimal strategies for measuring diffusion in anisotropic systems by magnetic resonance imaging. *Magn Reson Med* 42(3):515–525.
42. Zhu T, Liu X, Connelly PR, Zhong J (2008) An optimized wild bootstrap method for evaluation of measurement uncertainties of DTI-derived parameters in human brain. *Neuroimage* 40(3):1144–1156.
43. Wheeler-Kingshott C, Boulby P, Symms M, Barker G (2002) Optimized cardiac gating for high-resolution whole brain DTI on a standard scanner. *Proc Intl Soc Magn Reson Med Sci Meet Exhib* 10:1118.
44. Kerns JG, et al. (2004) Anterior cingulate conflict monitoring and adjustments in control. *Science* 303(5660):1023–1026.
45. Smith SM, et al. (2011) Network modelling methods for FMRI. *Neuroimage* 54(2): 875–891.
46. Harrison L, Penny WD, Friston K (2003) Multivariate autoregressive modeling of fMRI time series. *Neuroimage* 19(4):1477–1491.
47. Jezzard P, Balaban RS (1995) Correction for geometric distortion in echo planar images from B0 field variations. *Magn Reson Med* 34(1):65–73.
48. Behrens TE, et al. (2003) Non-invasive mapping of connections between human thalamus and cortex using diffusion imaging. *Nat Neurosci* 6(7):750–757.
49. Behrens TE, et al. (2003) Characterization and propagation of uncertainty in diffusion-weighted MR imaging. *Magn Reson Med* 50(5):1077–1088.
50. Croxson PL, et al. (2005) Quantitative investigation of connections of the prefrontal cortex in the human and macaque using probabilistic diffusion tractography. *J Neurosci* 25(39):8854–8866.

Supporting Information

Szczepanski et al. 10.1073/pnas.1313903110

SI Materials and Methods

Experimental Design. ***Motion detection task.*** Trials for the attended condition began with a 100% valid centrally presented cue to either the right visual field (RVF) or left visual field (LVF). After a variable expectation period (3.2–9.6 s long), moving, chromatic dot patterns (100 dots moving at 7°/s in 2.8 × 2.8° aperture) appeared at 10.8° eccentricity from fixation in the upper visual field of the cued side. Dots moved in one of four directions, changing direction every 400 ms. We set the motion coherence of dots to 10% above each individual subject's threshold for dot motion coherence in the periphery, calculated by using a staircase procedure before scanning. The direction of the first moving dot pattern became the target motion for that block. Subjects subsequently responded, by pressing a button, when that target motion reappeared. Because the subjects needed to identify the first brief motion stimulus that appeared on the screen to identify future repeats, subjects would be unable to perform the motion detection task if they were not paying attention to this first stimulus. When the moving dots disappeared, a tone prompted subjects to covertly shift their attention back to fixation. Each trial ended with a rest period.

Trials for the unattended condition had identical timing (Fig. 1*A*) and visual stimulation, except there was no cue at trial onset. In the unattended condition, the motion stimuli still appeared in the periphery, but subjects ignored the stimuli and instead maintained fixation on a central cross and responded when the cross briefly changed luminance.

Pattern detection task. We presented four colorful, complex images, each a 2° × 2° "tile," in adjacent locations, arranged as a large square, at 8–12° eccentricity from the fixation point to one of the visual field quadrants (a schematic outline of one run is shown in Fig. 2*A*). We presented tiles simultaneously for 250 ms, at 1 Hz, in 16-s blocks, with a temporal jitter of 250–750 ms (Fig. 2*A*, frames 2 and 5). We randomized the order of the tiles, their locations within the large square, and the quadrant in which tiles appeared. In the attended condition, a 500-ms, 100% valid cue (onset 1 s before tiles; frame 4) at fixation instructed subjects to covertly direct attention to one of the four peripheral locations and to count the occurrences of a target stimulus in the location closest to fixation (frame 5). Importantly, the target location was represented in gaze-centered coordinates (relative to fixation) and in object-centered coordinates (relative to the large square) that differed in field sign (e.g., when subjects directed attention to the right hemifield, the target was represented on the left side of the large square). Subjects reported the number of targets that appeared in each location at the end of each scanning run.

In the unattended condition (frame 2), the identical visual stimuli appeared in the periphery, but subjects were not cued to attend to these stimuli. Instead, subjects performed a demanding rapid serial visual presentation task at fixation, counting the number of target letters among distracters, while ignoring the peripherally presented stimuli.

We asked subjects after the scanning session what they perceived while preforming the pattern detection task and they reported the perception that all four tiles were part of the same object (1).

Visual Display. We generated visual displays on a Macintosh computer (Apple Computer) by using MATLAB software (MathWorks) and Psychophysics Toolbox functions. A PowerLite 7250 liquid crystal display projector (Epson) outside the scanner room displayed the stimuli onto a translucent screen located at the end of the scanner bore. Subjects viewed the screen at a total path length of 60 cm through a mirror attached to the head coil. The screen subtended 30° of visual angle in the horizontal dimension and 26° in the vertical dimension. A trigger pulse from the scanner synchronized the onset of stimulus presentation to the beginning of the image acquisition.

Data Analysis. ***Software.*** We analyzed data by using the AFNI software package, FreeSurfer, SUMA (http://afni.nimh.nih.gov/afni/suma), MATLAB, program 1dGC (http://afni.nimh.nih.gov/sscc/gangc/1dGC) in R (2), and FSL.

Defining ROIs. All functional images underwent a rigid motion-correction procedure to the image acquired closest in time to the anatomical scan (3). After motion correction, we geometrically unwarped images by using a field map and magnitude image acquired in the same session (4). We smoothed data with a 4-mm Gaussian kernel and normalized each time series to its mean intensity.

We performed a multiple regression analysis for the motion and pattern detection tasks. Square-wave regressors matching the timecourse of the design were identified as regressors of interest. We convolved each regressor with a gamma-variate function to best represent the idealized hemodynamic response. For the motion detection task, attention-related activity in frontoparietal cortex was defined by contrasting the expectation period and the visually evoked activity during all attended trials with the visually evoked activity during unattended trials. We used the same contrast to define the frontoparietal attention network for the pattern detection task, except only the visually evoked activity during the attended blocks was contrasted with unattended blocks. We thresholded statistical maps at an F score of 10.80 ($P < 0.001$, uncorrected for multiple comparisons).

We defined topographic areas frontal eye field (FEF), intraparietal sulcus areas 1–5 (IPS1–IPS5) and superior parietal lobule area 1 (SPL1) in each subject ($n = 21$) by using a memory-guided saccade task: Subjects performed delayed saccades to peripheral locations arranged clockwise around a central fixation point (5, 6). We identified the voxel with the peak attention activity in each topographic area of each hemisphere and created an ROI consisting of the peak attention voxel and the six surrounding voxels in the x, y, and z directions. We identified the supplementary eye field (SEF) based on anatomical and functional characteristics (6) and created an ROI consisting of the peak attention voxel and the six surrounding voxels. We used these ROIs for the functional connectivity analyses.

For the diffusion tractography analyses, we defined bilateral masks for IPS2 and SPL1 (seed areas) and bilateral masks for FEF and SEF (target areas). We defined ROIs as voxels at the intersection between the attention activations and each topographic map or, for SEF, as all voxels activated by attention.

Eye Movement Recordings. We monitored eye movements during scanning sessions in 11 of 14 subjects performing the memory-guided saccade task, in five of eight subjects performing the motion detection task, and in all subjects performing the pattern detection task. The remaining subjects could not be eye-tracked because of technical issues at the time of the scan session. We used a stimulus screen with a hole of 1.9° in diameter located at one edge through which a subject's eye was viewed with the help of a telephoto lens (Model 504 with Long Range Optics; Applied Science Laboratories). The eye position was displayed in real time on a video monitor in the scanner control room, superimposed

on the stimulus image. The experimenter observed the eye position display to ensure that the subjects were alert and performing the appropriate task, which was to either make a saccade in the correct direction during the memory-guided saccade task or to maintain fixation throughout the motion and pattern detection tasks. We recorded eye position data on the stimulus computer through a serial interface with the eye-tracker control module. The eye tracking system, which measured the eye position at a rate of 60 Hz, had a resolution of ~0.10°, and detected differences in relative eye position of ~0.50°.

We used Ilab software (7) to analyze the eye movement data. For both attention tasks, we calculated separate frequency histograms of the vertical and horizontal eye position data for each subject. Data were collected and analyzed separately for periods of covert attention to each quadrant within the visual field and for periods when stimuli were presented, but subjects were not attending peripherally. We then used two-sample t tests to determine whether eye movements systematically deviated in any direction during attention to any of the four quadrants. Additionally, we defined one eye movement region (EMR), $1° \times 1°$ in size, around the central fixation cross and calculated the number of times the gaze left this EMR. See ref. 4 for analysis details. The maximum difference in mean horizontal and vertical eye positions among the experimental conditions was 0.12 and 0.06 degrees, respectively. There were no systematic horizontal or vertical eye deviations between any of the different experimental conditions (all $P > 0.20$). Fixation was well maintained and almost never left the EMR surrounding the central fixation cross. Of the horizontal and vertical position samples, 97.6 ± 0.5% (mean, SEM) were within the EMR during a given scan session. This analysis confirms that subjects maintained fixation throughout trials/blocks and did not shift their gaze location along with attention.

1. Blake R, Lee SH (2005) The role of temporal structure in human vision. *Behav Cogn Neurosci Rev* 4(1):21–42.
2. Pfaff B (2008) VAR, SVAR and SVEC models: Implementation within R package vars. *J Stat Softw* 27(4):1–32.
3. Cox RW, Jesmanowicz A (1999) Real-time 3D image registration for functional MRI. *Magn Reson Med* 42(6):1014–1018.
4. Jezzard P, Balaban RS (1995) Correction for geometric distortion in echo planar images from B0 field variations. *Magn Reson Med* 34(1):65–73.
5. Sereno MI, Pitzalis S, Martinez A (2001) Mapping of contralateral space in retinotopic coordinates by a parietal cortical area in humans. *Science* 294(5545):1350–1354.
6. Szczepanski SM, Konen CS, Kastner S (2010) Mechanisms of spatial attention control in frontal and parietal cortex. *J Neurosci* 30(1):148–160.
7. Gitelman DR (2002) ILAB: a program for postexperimental eye movement analysis. *Behav Res Methods Instrum Comput* 34(4):605–612.

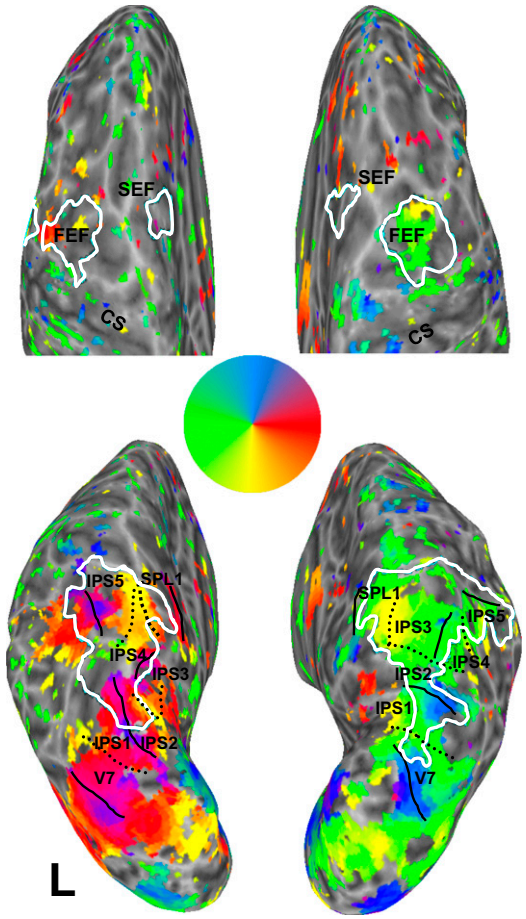

Fig. S1. Posterior parietal cortex (PPC) areas and FEF show topographic organization, whereas SEF does not. Topographic maps in frontal (*Upper*) and parietal (*Lower*) cortex from a representative subject, obtained using the memory-guided saccade task and projected onto an inflated surface of the subject's brain. The color legend represents the saccade direction/memorized location to which voxels most respond. Boundaries between PPC areas are marked by black lines, with continuous lines denoting the upper vertical meridian, and broken lines denoting the lower vertical meridian. White lines define the extent of the attention activations (attended vs. unattended, $P < 0.001$) in the same subject while performing the motion detection task. IPS1-5, SPL1, and FEF showed topographic organization and also contained attention-activated voxels. There was no evidence of topographic organization in the SEF, even when activity from the memory-guided saccade task was set to a liberal threshold (as shown), but the SEF was still significantly activated by the motion detection task. CS, central sulcus.

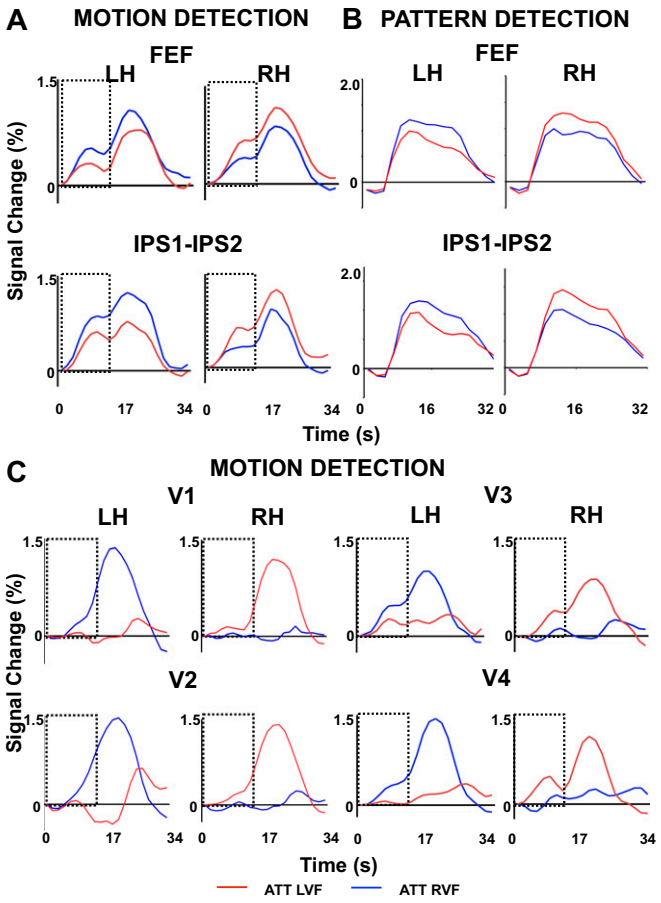

Fig. S2. Focused spatial attention effects on blood oxygen level-dependent (BOLD) responses from individual frontoparietal and visual areas. (*A*) Averaged BOLD timecourses from frontal (FEF; *Upper*) and parietal (mean of IPS1 and IPS2; *Lower*) areas while subjects attended either to the RVF or the LVF during the motion detection task. (*B*) Averaged BOLD timecourses from the same areas while subjects attended either to the RVF or the LVF during the pattern detection task. (*C*) Averaged BOLD timecourses from V1, V2, V3, and V4 while subjects performed the motion detection task. The dotted box around the timecourses in *A* and *C* defines the expectation period (when subjects allocated attention in the absence of visual stimuli).

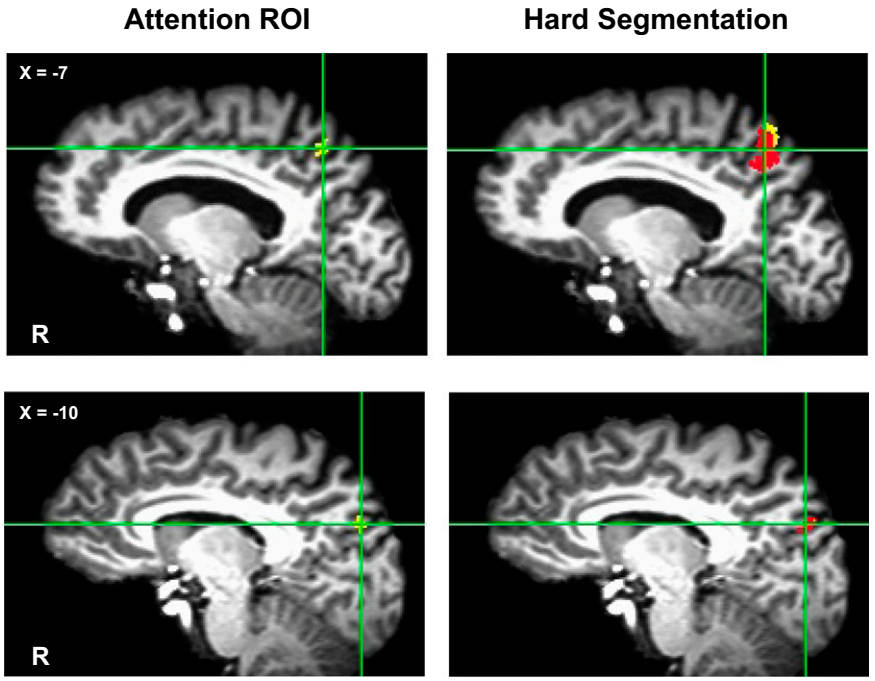

Fig. S3. Overlap between SPL1 voxels functionally connected with SEF and SPL1 voxels structurally connected to SEF. (*Left*) Peak attention ROIs (yellow voxels) in SPL1 of two example subjects (*Upper* and *Lower*). (*Right*) Corresponding hard segmentation of SPL1 in the same subjects. Red voxels in SPL1 project to the SEF, whereas yellow voxels project to the FEF.